Size and Catalytic Activity of Supported Gold Nanoparticles: An in Operando Study during CO Oxidation

ARTICLE *in* THE JOURNAL OF PHYSICAL CHEMISTRY C · MARCH 2011

Impact Factor: 4.77 · DOI: 10.1021/jp1110554

10 AUTHORS, INCLUDING:

Jacques Jupille
Pierre and Marie Curie University - Paris 6
156 PUBLICATIONS **2,618** CITATIONS
SEE PROFILE

O. Robach
Atomic Energy and Alternative Energies Com…
73 PUBLICATIONS **992** CITATIONS
SEE PROFILE

Gregory Cabailh
Pierre and Marie Curie University - Paris 6
32 PUBLICATIONS **564** CITATIONS
SEE PROFILE

Aude Bailly
French National Centre for Scientific Research
29 PUBLICATIONS **280** CITATIONS
SEE PROFILE

THE JOURNAL OF PHYSICAL CHEMISTRY C

ARTICLE

pubs.acs.org/JPCC

Size and Catalytic Activity of Supported Gold Nanoparticles: An in Operando Study during CO Oxidation

I. Laoufi,[†] M.-C. Saint-Lager,[*,†] R. Lazzari,[‡] J. Jupille,[‡] O. Robach,[§] S. Garaudée,[†] G. Cabailh,[‡] P. Dolle,[†] H. Cruguel,[‡] and A. Bailly[†]

[†]Institut Néel, CNRS et Université Joseph Fourier, BP 166, F-38042 Grenoble Cedex 9, France

[‡]Institut des NanoSciences de Paris, Université Pierre et Marie Curie Paris 6, UMR 7588 CNRS, 4 place Jussieu, F-75252 Paris Cedex 05, France

[§]Institut Nanosciences et Cryogénie, Commissariat à l'Energie Atomique et aux Energies Alternatives, 17 avenue des Martyrs, F-38054 Grenoble Cedex 9, France

ABSTRACT: The origin of the catalytic activity of gold nanoparticles remains debated despite extensive studies. This in operando work investigates the relationship between catalytic activity and size/shape of gold nanoparticles supported on $TiO_2(110)$ during CO oxidation. The nanoparticles were synthesized by vapor deposition in ultrahigh vacuum. Their geometry was monitored in the presence of O_2, Ar, or a mixture of O_2 + CO and of Ar + CO by grazing incidence small-angle X-ray scattering simultaneously with the catalytic activity. The occurrence of CO oxidation induces a sintering directly correlated to the reaction rate. The catalytic activity is optimum for a nanoparticle's diameter of 2.1 ± 0.3 nm and a height of about six atomic layers. Below this size, the activity drop corresponds to a height decrease. Rescaling of activities obtained in different experimental conditions shows consistency of these results with published data using both "model" and "real" catalysts.

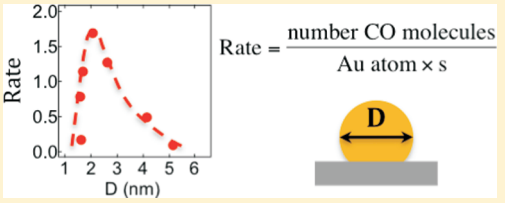

INTRODUCTION

The extraordinary catalytic activity of supported gold nanoparticles has generated great excitement over the last two decades. Under conditions in which the bulk metal is barely active, dispersed gold was shown to catalyze a great number of reactions.[1−3] The interest of researchers was particularly focused on the carbon monoxide (CO) oxidation especially because gold catalyzes this reaction at temperatures as low as 200 K[4] with an even better activity than platinum.[5] Therefore, gold nanoparticles offer promising solutions for a use in mild conditions for either gas sensing[6] or gas purification,[1] including preventing the poisoning of platinum in proton exchange membrane fuel cells.[7]

There exists a large consensus that active gold involves particles smaller than about 5 nm in size.[2] However, the origin of this catalytic activity is still controversial. Haruta et al. first suggested that the reaction takes place at the interfacial perimeter around the gold nanoparticle,[8] a view recently supported by a study of the oxygen storage capacity of Au/TiO_2.[9] Instead, Nørskov et al. favored corners as active sites.[10,11] On the basis of density functional theory (DFT) calculations, and in line with previous papers,[12] they claimed that the low-coordinated Au atoms play a major role in the catalytic activity. Several published works support this hypothesis, such as the study of the size dependence of gold reactivity by extended X-ray absorption fine structure experiments (EXAFS).[13] Alternatively, Goodman et al. assigned the catalytic properties to a quantum size effect peaking for two-atom-thick gold clusters with diameters ranging from 2.5 to 3 nm in size.[14] More recently, by examining the activity of well-ordered wetting gold films, they showed that a bilayer feature was critical for the catalytic activity.[15,16] The role of subnanometer Au clusters in the reactivity is also discussed. Indeed, the catalytic activity of iron oxide-supported gold catalysts was found to stem from particles as small as 0.5 nm in diameter with ca. 10 atoms per cluster using aberration-corrected transmission electron microscopy (TEM).[17]

Haruta et al. first showed that the reactivity of gold nanoparticles sharply increases when the diameter decreases below 4 nm.[8] Later, Valden and Goodman highlighted the existence of an optimum diameter around 3 nm for which the activity was maximum.[14] They relied on their work performed on model catalysts prepared by vapor deposition in ultrahigh vacuum (UHV) and on the values previously published by Bamwenda et al. obtained on chemically synthesized catalysts.[5] Thereafter, others studies, exploring the sizes smaller than 2 nm, also pointed out a maximum in activity.[18,19] However, the interpretation, which assigns this maximum to clusters with a height of two atomic layers,[14,16] remains controversial. For instance, the observation of a constant CO stretching frequency on two-dimensional gold films of various thicknesses argues against a specific reactive behavior of one- and two-monolayer-thick gold films with respect to bulk gold.[20] In addition, in situ X-ray photoelectron spectroscopy measurements indicate that, under reaction conditions, gold remains in the metallic state.[21] Moreover, the height of the nanoparticles at the maximum of reactivity was found to be five to seven atomic layers, as observed by

Received: November 19, 2010
Revised: February 1, 2011
Published: March 03, 2011

high-resolution TEM,[18] instead of two, as claimed by Goodman et al.[14,16]

The various forms of gold, from three-dimensional nanoparticles[1,4,5,18,19] to ultrasmall clusters[17] or two-layer-thick particles,[14] proposed to explain its extraordinary catalytic activity make the question of the relationship between the particle features (morphology and size) and the catalytic activity more pressing than ever. However, none of the studies up to now were performed by measuring the geometrical parameters of the particles simultaneously with the catalytic activity. Such operando studies are of paramount importance because, very often, the nanoparticles sinter in the course of the catalytic reaction. The sintering rate greatly depends on the nanoparticle preparation conditions and on the sample history. It is usually important for model catalysts prepared in UHV, and it is associated with nanoparticles deactivation.[22] For dispersed catalysts, temperature reduction and a calcination procedure are used to stabilize the particles,[23] but, in return, they become larger and less reactive. The sintering is greater when the particles are initially small;[24] such particles being more difficult to stabilize. Therefore, the sintering effect can become an issue around the optimum size for catalytic activity and below.

The present paper reports on the catalytic activity measurements of Au/TiO_2(110) nanoparticles during CO oxidation. A titania support was chosen because it is a test bed[1−3] to study gold catalysts synthesized both in UHV[14] and by chemical methods.[1,4,5,18,19] Reactivity measurements and grazing incidence small-angle X-ray scattering (GISAXS) were simultaneously performed in a dedicated system, bridging the "pressure gap" between surface science and realistic reaction conditions,[25,24] for particles size down to 1 nm.

EXPERIMENTAL METHODS

The setup consists of an UHV preparation chamber and a batch reactor running from UHV to reactive conditions at ambient pressures and allowing both X-ray scattering and activity measurements in static conditions.[24,25] The setup was installed at the European Synchrotron Radiation Facility (ESRF) on beamline BM32 to perform this experiment.

The TiO_2(110) crystal was prepared in UHV by ion bombardment, followed by annealing at 1000 K under an oxygen partial pressure of 10^{-3} Pa to restore the surface stoichiometry.[26] Gold nanoparticles were grown by vapor deposition at 300 K in UHV (base pressure = 5×10^{-8} Pa). As calibrated by a quartz microbalance, the average thickness of the gold deposit was ranging between 0.05 and 3 monolayers (1 ML corresponding to 0.235 nm, equivalent to one Au(111) atomic layer). Once prepared, the Au/TiO_2(110) samples were transferred into the reactor under UHV for GISAXS and catalytic activity measurements.

Because the morphology of the particles is dependent on the gas environment and on the history, the exposure to reactive gases was always performed according to the same protocol throughout the study. It involved three steps, each lasting approxi-
mately 2 h, during which GISAXS and gas composition were measured: (1) Au/TiO_2(110) was inserted in the reaction chamber under UHV, (2) then annealed at 473 K under 2×10^3 Pa of oxygen, (3) and CO conversion into CO_2 started by adding 20 Pa of CO to the oxygen, while keeping the sample at 473 K. This procedure allows distinguishing the effect induced by the reaction itself from the one due to oxygen pressure or annealing. Moreover, some measurements were also performed by replacing oxygen with argon. To establish the relationship between particle size and catalytic activity, the average geometry of the particles was determined from GISAXS patterns recorded during the same lapse of time as the reactivity, that is, during the first 10 min of step (3).

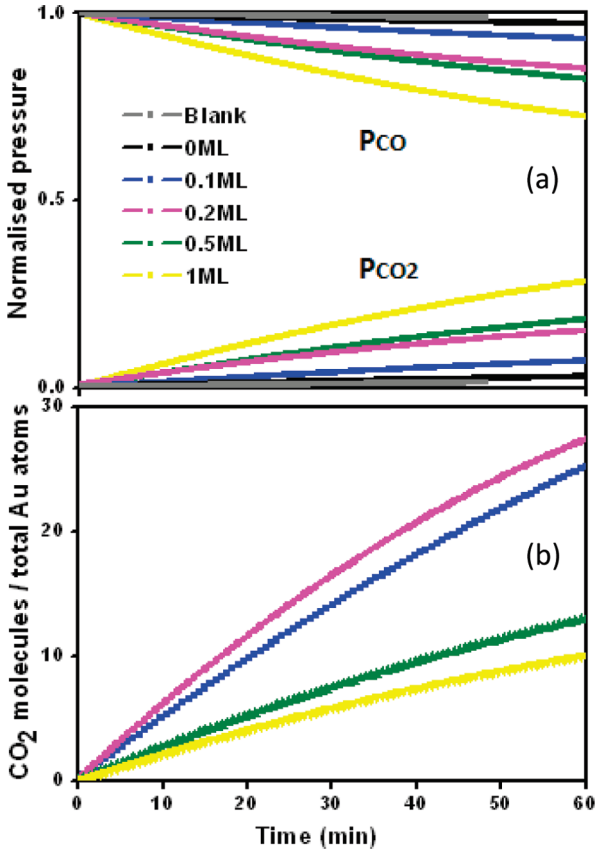

Figure 1. (a) Time evolution of the CO and CO_2 partial pressures (normalized to the CO pressure at $t = 0$) as deduced from the mass spectrum signal for several gold deposits. The gray curve corresponds to the residual CO conversion of the sample holder (blank) without substrate, the black one to the clean TiO_2(110) substrate, and the other ones to different gold equivalent thicknesses expressed in monolayer (ML). The upper curves correspond to the consumption of CO and the lower ones to the production of CO_2 in the batch reactor. (b) Time evolution of the number of CO_2 molecules produced by CO conversion derived from the partial pressure of (a) after subtracting the background and normalization to the deposited gold amount.

As indicated, the catalytic activity was measured after adding 20 Pa of CO in 2×10^3 Pa of oxygen at 473K. These conditions of "low" CO pressure and "high" temperature were chosen to detect the activity of this small area catalyst, which consists of a fraction of a Au monolayer on a 1×1 cm^2 substrate. Moreover, the detection of the GISAXS patterns of such small particles needs the addition of guard slits inside the reactor,[27] yielding a large volume.[24] The CO and CO_2 partial pressures in the reactor chamber are deduced from the 28 and 44 m/e ionization currents as measured by a mass spectrometer.[24,25] The evolutions of the normalized partial pressures $P_{CO}(t)$ and $P_{CO_2}(t)$ are shown in Figure 1a for several amounts of deposited gold. The detection limit is given by the spurious reactivity mainly due to the heated sample holder. As shown in Figure 1a, the reaction rate for 0.1

dx.doi.org/10.1021/jp1110554 |J. Phys. Chem. C 2011, 115, 4673–4679

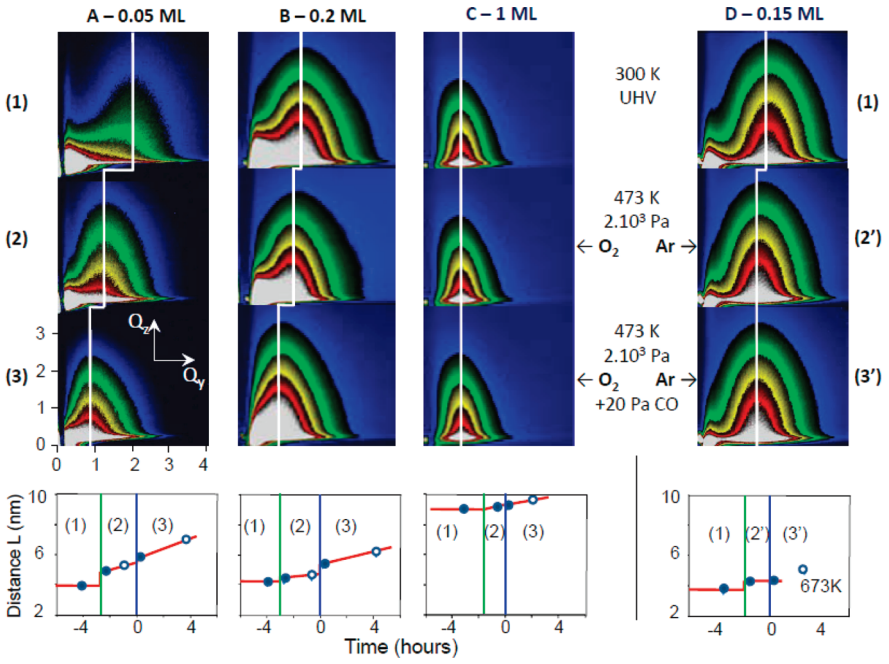

Figure 2. GISAXS patterns recorded from Au/TiO_2(110) nanoparticle assemblies with an X-ray beam along the $[110]_{TiO_2}$ direction (only one of the two lobes is shown). Each column represents a different sample characterized by its gold coverage. Each row corresponds to a given step of the gas/temperature environment as defined in the text. For each image, the coordinates in nm^{-1} are the wavevector transfers Q_y and Q_z that are, respectively, parallel and perpendicular to the substrate surface. The intensity scale is logarithmic and is the same for all the patterns of a given sample. The white lines indicate Q_M, the position of the correlation peak. Bottom: for each sample, diagram showing the evolution of the interparticle distances L as derived from the correlation peak position; filled (empty) circles correspond to patterns (not) shown in the figure. For sample D, further annealing to 673 K was performed.

ML of gold, corresponding to a catalyst amount as low as 50 ng, is well above the sensitivity limit. Figure 1b corresponds to the number of CO_2 molecules derived from $P_{CO_2}(t)$ curves of Figure 1a and normalized by the gold amount deposited in each case. It allows one to see that the 0.2 ML gold deposit is actually the most reactive. To reduce the exposure time to X-ray photons, which can affect the reaction,[28] a beamshutter controlled the illumination of the sample. We checked that the activity was the same with and without the X-ray beam.

The reaction rate was defined as the number of CO molecules converted per gold atom per second on the basis of the total number of gold atoms. It is calculated from the slope of the $P_{CO}(t)$ curve during the initial 10 min of the reaction and after subtraction of the background signal.

Operando GISAXS Measurements. GISAXS measurements involve the recording of the intensity scattered by the assembly of particles in a plane perpendicular to the sample surface around the direct X-ray beam and on both sides of the reflected beam (see Figure 2). The presence of a well-defined lobe, called a correlation peak, indicates that particles are regularly distributed on the substrate surface. The GISAXS patterns were recorded in the same conditions as in ref 24. The quantitative analysis procedure used for a given scattering pattern was already descr ibed in the literature.[29] Only the relevant hypotheses are summarized below. Data were recorded with incidence and emergence angles close to the critical angle (0.13° at the photon energy of 18 keV) to enhance the nanoparticles' GISAXS signal. To take into account the reflection and refraction effects, the particles form factor was calculated in the frame of the so-called distorted-wave born approximation (DWBA)[30,31,29] for diluted systems.[32] It was averaged over a Gaussian size distribution while a paracrystalline interference function was used to describe the in-plane disorder of the particles collection.[33] The scattering cross section was treated in the well-known local monodisperse approximation of Pedersen et al.[34,29] This analysis gives the mean values of the size distribution (particles height, H; diameter, D; and separation distance, L) derived by modeling gold particles by truncated spheres.[32,24]

To determine the geometry of the particles with a good accuracy down to coverages of gold as low as 0.05 ML, several intensity profiles of the GISAXS patterns (as shown in Figure 3) were simultaneously fitted with the *IsGISAXS* software.[31] One profile was taken along the Q_z direction across the correlation peak (i.e., at the maximum of the lobe intensity, as illustrated by the white line on the GISAXS patterns in Figure 2). The other profile was taken along the direction Q_y, but in the case of a low intense GISAXS signal, it is perturbed by the tail of the specular rod (see Figure 2, close to $Q_y = 0$). This contribution, due to the substrate roughness, was excluded from the fit. To increase statistics and constrain the model, several cuts along Q_y were used, up to Q_z values for which this disturbance becomes negligible. To improve the accuracy, the obtained geometrical parameters were averaged over fits of patterns acquired with the incident beam along the two main TiO_2(110) surface directions: [110], along the oxygen rows, and [001], perpendicularly to them.[35] The same shape was found in these two directions, whereas the interparticle distance L was larger along the [110] direction than along [001].

RESULTS

Sintering under Reactive Gases. An overview of the recorded GISAXS patterns is given in Figure 2. They are shown for

dx.doi.org/10.1021/jp1110554 |J. Phys. Chem. C 2011, 115, 4673–4679

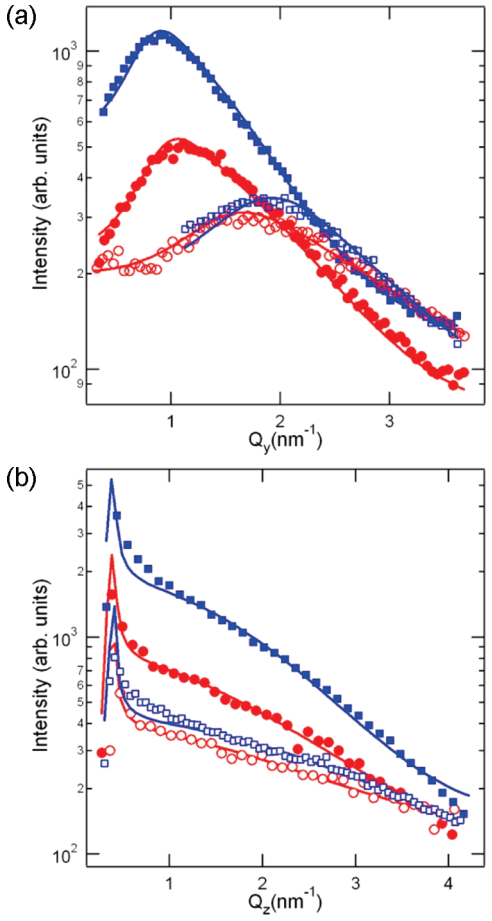

Figure 3. (a) Q_y cut of the GISAXS patterns at $Q_z = 1.66$ nm^{-1} and (b) Q_z profile at the maximum of the correlation peak. Red circles represent sample A (0.05 ML) and the blue squares sample E (0.1 ML); empty and filled dots are associated with patterns recorded in UHV at 300 K (step 1) and under 2×10^3 Pa O_2 + 20 Pa CO at 473 K at the beginning of step 3, respectively. The full lines are the fitted curves obtained with particles modeled by size distributed truncated spheres with the geometrical parameters given in Table 1.

three representative samples, A, B, and C—corresponding to Au coverages of 0.05, 0.2, and 1 ML, respectively—during the three steps of the experiment. For sample D (0.15 ML), oxygen was replaced with argon. In UHV (step 1), the tendency of GISAXS patterns to shrink and shift toward the origin of the reciprocal space from A to C is consistent with particles increasing in size with a smaller cluster density as gold coverage increases. Gold particle morphology at 300 K is stable with time in UHV, as observed by GISAXS during 6 h on a 0.1 ML gold coverage (not shown). As a general trend, annealing and exposure to reactive gases produce a shift toward $Q_y = 0$ of the position of the correlation peaks at $Q_y = Q_M$ (marked by the white line in Figure 2). To the first approximation, Q_M can be directly linked to the mean separation distance L of the particles on the substrate by $L = 2\pi/Q_M$.[36] Because the system evolves with a constant amount of gold on the TiO_2 substrate, the increase of L is a clear signature of sintering, which also involves an increase of the mean diameter D and height H of the particles. The corresponding evolution of L is plotted on the graphs of Figure 2 at the bottom of the series of patterns for each sample. Annealing from 300 to 473 K results in an increase of L depending on the initial

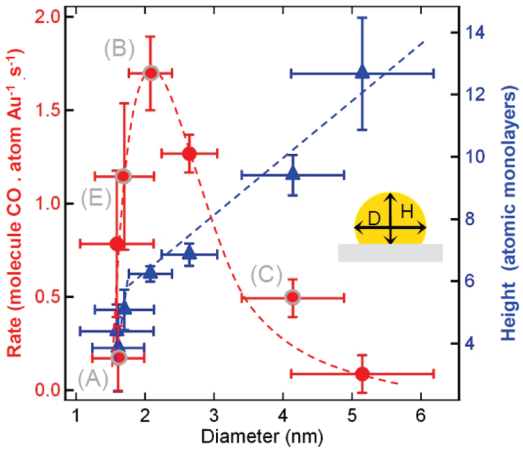

Figure 4. Reaction rate as a function of the mean particle diameter (red circles). The labels correspond to the different samples mentioned in the text. Blue triangles: variation of the measured mean height (in number of atomic layers) as a function of the diameter. The dashed lines are guide for eyes, and the error bars represent the width of the size distribution.

gold amount. The change is large for the lowest amount, which corresponds to the smallest particles (sample A), is less important when the size increases (sample B), and becomes negligible above a coverage of 1 ML (sample C). Moreover, this effect hardly depends on the presence of oxygen, as seen by comparing sample B (step 1 to 2) to sample D, with roughly the same gold coverage but under argon instead of oxygen (step 1 to step 2′). Therefore, this sintering seems thermally activated.

The occurrence of the catalytic reaction that follows the introduction of CO in the presence of oxygen (step 2 to step 3) clearly affects the morphology of the particles, as shown in the graphs of Figure 2; the change also depends on the gold coverage with a sudden increase of L observed for samples A and B when CO is introduced. Noticeably, the greatest increase of the interparticle distance is not observed for the smallest particles (sample A) but for the particle size at the maximum of activity (see sample B in Figure 4). For the biggest particles (sample C), there is almost no evolution. The addition of CO within argon at 473 K had no effect at all (sample D: step 2′ to step 3′), whereas annealing sample D in inert conditions (step 3′) activates the sintering (Figure 2, bottom). The sintering acceleration occurring consecutively to CO introduction is thus clearly induced by the oxidation reaction. This latter being highly exothermic, the sintering may be a consequence of a local heating effect, as already suggested,[37] but it may also result from a more complex reactant-induced mass transport mechanism.[38] After a very short transition time (less than 1 min), the sintering slows down, allowing measurements under almost stationary conditions over a time scale of 10 min as used to establish the size dependence of the activity.

Determination of the Geometrical Parameters. Quantitative analysis of GISAXS patterns provides a detailed description of the particle geometry in gaseous environments. Figure 3a,b illustrates the evolution of two significant cuts of the GISAXS patterns for samples with the lowest gold coverages: sample A, 0.05 ML; sample E, 0.1 ML, for which the sintering is the most important.

Table 1 sums up the main parameters deduced from the fits of GISAXS patterns obtained in UHV and under reaction conditions at the beginning of step 3. For both samples, the mean

Table 1. Geometrical Parameters, As Deduced from Fitting the GISAXS Pattern Profiles, for Sample A (0.05 ML) and Sample E (0.1 ML)[a]

coverage		D (nm)	$\Delta D/D$	H (nm)	H (ML)
0.05 ML	UHV	0.8	0.7	0.4	2 ± 2
	reaction	1.6	0.4	0.9	4 ± 1.5
0.1 ML	UHV	1.0	0.6	0.6	3 ± 1
	reaction	1.7	0.4	1.2	5.5 ± 1

[a] The height H is also given in number of atomic monolayers.

diameter of the nanoparticles is close to 1 nm in UHV. For sample A, the mean height is two atomic monolayers, but with a wide dispersion consistent with STM images.[39] This indicates that most of the nanoparticles have a pronounced quasi-2D character. Indeed, the coverage is below the critical value of ~0.1 ML, which was found as a limit for the 2D growth of $Au/TiO_2(110)$ at room temperature.[40,41] Moreover, Rashkeev et al. showed images of Au nanoparticles supported on anatase using Z-contrast scanning transmission electron microscopy (STEM).[42] For the most active form of the nanoparticles, obtained after a mild reduction in hydrogen, they found that the Au nanoparticles are mainly one or two layers thick, in accordance with our present finding. For sample E, with a slightly higher coverage, the mean nanoparticle height is about 3 ML. In reactive conditions at 473 K, the size of the gold nanoparticles shifts to higher values. The mean diameter expands similarly for the two samples and becomes about twice larger (1.6 ± 0.3 and 1.7 ± 0.3 nm for samples A and E, respectively). The height increases in a slightly different way for samples A and E (0.9 ± 0.3 and 1.2 ± 0.15 nm, respectively). The mean volume per island increases, evolving toward a shape closer to the equilibrium shape.[43] The 2D and smallest 3D clusters disappear, leaving a place to an assembly of bigger 3D nanoparticles with a narrower size distribution, as already observed by STM.[38] At a higher gold coverage (>0.15 ML), particles are already 3D when deposited.[39] Nevertheless, for coverages up to 1 ML, they undergo a noticeable increase of the mean size in the presence of the reactive mixture (Figure 3). These dramatic changes in the particles' morphology show that the size dependence of the catalytic activity requires an operando determination, by measuring simultaneously the catalytic activity and the particles' geometrical parameters.

Size Dependence of the Reactivity. The dependence of the catalytic activity on the particle size is presented in Figure 4. The activity increases as the diameter of the gold particles decreases below 5−6 nm. It passes through a maximum at 2.1 ± 0.3 nm where the height of the particles is six atomic layers. This maximum actually corresponds to a deposited gold amount of 0.2 ML, a deposit that was expected to be the most reactive, according to Figure 1b. Below the optimum diameter, the drop of the reactivity is abrupt. It also corresponds to a noticeable decrease in the height of the nanoparticles from 6 to less than 4 ML.

DISCUSSION

The present variation of the catalytic activity versus size, obtained with model catalysts prepared in UHV, was compared to already published works for supported gold prepared by various chemical ways, such as deposition-precipitation, followed by calcinations,[5,18] or deposition of colloidal gold particles of a controlled size on titania-coated silica aerogel.[19] The curve from Valden et al.,[14] who studied $Au/TiO_2(110)$ prepared in an UHV environment, is also reported. As all these experiments were performed in very different conditions of temperature and of oxygen (P_{O_2}) and CO (P_{CO}) partial pressures, a rescaling was performed according to

$$\mathrm{Rate}(D, T, P_{CO}, P_{O_2}) = \mathrm{rate}(D) \times P_{CO}^{\nu_{CO}} \times P_{O_2}^{\nu_{O_2}} \times \exp^{(-\Delta E/kT)} \quad (1)$$

To do so, it is assumed that the reaction orders ν_{CO} and ν_{O_2}, the activation energy ΔE, and the size dependence are nearly constant in the spanned thermodynamic ranges. The values $\nu_{CO} = 0.34$ and $\nu_{O_2} = 0.32$ given by Schumacher et al.[44] were used as their experimental conditions almost match the ones of the studies under comparison. Indeed, these values were determined for gold particles of 2.7 nm, a size close to the one at the maximum of activity. Moreover, the explored pressure range (from 40 to 4×10^3 Pa and 20 to 2×10^3 Pa for oxygen and CO, respectively) almost covers the pressures of the studies under concern. In addition, the working temperature of 353 K is an intermediate between the various experiments. The value ΔE of the activation energy for CO oxidation ($26\ \mathrm{kJ \cdot mol^{-1}}$) was taken as an average between the values previously published.[5,19,44] The extrapolation with eq 1 of the reaction rate determined by Schumacher et al., with $P_{CO} = 1 \times 10^3$ Pa and $P_{O_2} = 3 \times 10^3$ Pa. (Figure 1c of ref 44), to the pressure and temperature conditions of the present work leads to 2.2 CO molecule·atom $Au^{-1} \cdot s^{-1}$, close to 1.7 CO molecule·atom $Au^{-1} \cdot s^{-1}$ found in the present work at the maximum of catalytic activity. This shows that the assumptions of eq 1 and the values used for the involved parameters are reasonable. After rescaling of data sets from the literature using eq 1, a great similarity is observed (Figure 5)

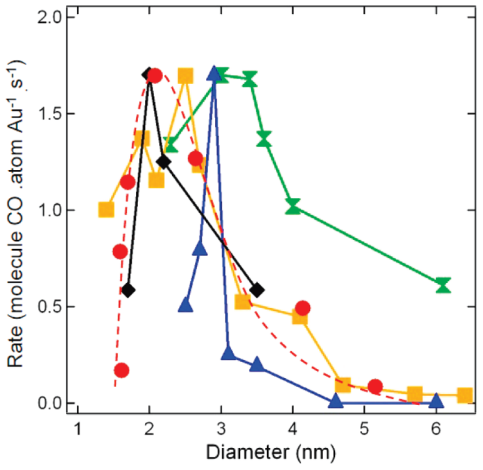

Figure 5. Comparison of the present data with previously reported experimental studies. All the data sets were extrapolated to the conditions of the present work by using eq 1 and were then normalized to the maximum of activity by using the rescaling factor α. Red points and dashed line (present work): $P_{O_2} = 2 \times 10^3$ Pa, $P_{CO} = 20$ Pa, and $T = 473$ K. Blue triangles (Bamwenda et al.[5]): $P_{O_2} = 2.1 \times 10^3$ Pa, $P_{CO} = 10^3$ Pa, $T = 273$ K, and $\alpha = 2.3$. Green crosses (Valden et al.[14]): $P_{O_2} = 4.4 \times 10^3$ Pa, $P_{CO} = 0.9$ Pa, $T = 350$ K, and $\alpha = 0.45$. Black diamonds (Zanella et al.[18]): $P_{O_2} = 4 \times 10^3$ Pa, $P_{CO} = 10^3$ Pa, $T = 278$ K, and $\alpha = 0.9$ (in that case, only the data prepared with NaOH and with 100% metallic gold were taken into account). Orange squares (Tai et al.[19]): $P_{O_2} = 2.1 \times 10^4$ Pa, $P_{CO} = 10^3$ Pa, $T = 300$ K, and $\alpha = 1.5$. In the latter case, $1.2/D$ was used as dispersion to convert the TOF given in ref 19 (defined per surface atom) into rate (per total Au atom).[23]

dx.doi.org/10.1021/jp1110554 |J. Phys. Chem. C 2011, 115, 4673–4679

despite the disparities between the experimental conditions. The most important discrepancy is observed with the curve obtained by Valden et al.[14] for model catalysts prepared in UHV but with geometrical parameters not determined directly under reactive conditions.

The diameter corresponding to catalytically active gold nanoparticles is in the range of 1−5 nm with a well-defined optimum that appears in a narrower range, between 2 and 3 nm. The existence of an optimal particle size, as first evidenced by Valden et al.,[14] is unambiguously confirmed. The present measurement of 2.1 ± 0.3 nm for the diameter agrees with their values of 3−3.5 nm, but in contrast to these authors, the particles are not found to be two atomic layers in height, but thicker with about six atomic planes, as it can be seen in Figure 4. The dimensionality of the particles at the maximum (i.e., 3D instead of 2D particles) is consistent with the result found on the dispersed catalyst.[18] This finding parallels the role of the reaction-induced sintering, which tends to modify the particle morphology toward a more rounded shape closer to the equilibrium. Moreover, Figure 4 evidences a drop of the activity for particle height below 5−6 atomic ML. These results argue against the existence of a "magic" bilayer model associated with the high reactivity of the supported gold nanoparticles.

An earlier paper pointed out the dominant role of extremely small clusters in order to explain the great catalytic activity of gold for CO oxidation.[17] In our case, the present data tend to rule out this assumption. Indeed, the existence of an optimal diameter of about 2 nm indicates that smaller particles are less active. Moreover, the sintering affecting mainly the smallest particles, as shown here (see samples A and B in Figure 2), tends to show that the smallest clusters disappear from the sample surface to the benefit of the biggest ones.

Regarding the actual value of the catalytic activity at the maximum, a scaling factor α close to 1 was applied to the results obtained in the various experiments (see Figure 5). Given the very different conditions used in these studies, the data recorded herein by operando studies on model catalysts can be representative of those recorded on "real" catalysts operated in normal conditions. Therefore, the conclusions drawn in the present work about the relationship between reactivity and particle size sketch an unified picture of the titania-supported gold catalyst.

CONCLUSION

In this paper, the relationship between the catalytic activity and the geometrical parameters of gold clusters supported on TiO_2(110) was studied in operando during CO oxidation. A reaction-induced sintering was clearly observed with a rate directly correlated to that of the CO oxidation. The sintering irreversibly changes the morphology of the active nanoparticles evolving toward a more rounded equilibrium shape. Active particles were found to be three-dimensional with a maximum in activity for a diameter of 2.1 ± 0.3 nm and a height of about six atomic planes. These findings were compared to other studies performed on catalysts prepared in very different conditions, including evaporation of gold on a crystal surface and impregnation−precipitation and deposition of colloidal gold. This demonstrated that operando studies on model catalysts in the frame of a surface science approach can be representative of applied catalysis. Maxima in reactivity have also been found for gold particles of 2.5−3 nm in size, in the case of the surface oxidation of silicon,[45] and, in liquid phase, in the case of the electrocatalytic oxidation of CO.[46] Because 2 nm is a critical diameter for noble metals, which corresponds to the loss of their intrinsic metallic nature,[47] further theoretical and operando experimental investigations of gold clusters with diameters around and below 2.0 nm will be needed to elucidate the mechanisms at work in the chemistry of gold catalysts.

AUTHOR INFORMATION

Corresponding Author

*Tel: (+33) (0)476 887 415. Fax: (+33) (0)476 881 038. E-mail: marie-claire.saint-lager@grenoble.cnrs.fr.

ACKNOWLEDGMENT

The technical staffs (SERAS and MCMF) of Institut Néel-CNRS and of the BM32 CRG beamline at ESRF are acknowledged for their help. This work was partly supported by funding ANR-07-NANO-024.

REFERENCES

(1) (a) Haruta, M. *Catal. Surv. Jpn.* **1997**, *1*, 61–73. (b) Haruta, M. *Catal. Today* **1997**, *36*, 153–166.
(2) Bond, G. C.; Thompson, D. T. *Gold Bull.* **2000**, *33*, 41–50.
(3) Meyer, R.; Lemire, C.; Shaikhutdinov, S. K.; Freund, H.-J. *Gold Bull.* **2004**, *37*, 72–124.
(4) Haruta, M.; Yamada, N.; Kobayashi, T.; Iijima, S. *J. Catal.* **1989**, *115*, 301–309.
(5) Bamwenda, G. R.; Tsubota, S.; Nakamura, T.; Haruta, M. *Catal. Lett.* **1997**, *44*, 83–87.
(6) Kobayashi, T.; Haruta, M.; Sano, H.; Nakane, M. *Sens. Actuators* **1988**, *13*, 339–349.
(7) Cameron, D.; Holliday, R.; Thompson, D. *J. Power Sources* **2003**, *118*, 298–303.
(8) Haruta, M.; Tsubota, S.; Kobayashi, T.; Kageyama, H.; Genet, M. J.; Delmon, B. *J. Catal.* **1993**, *144*, 175–192.
(9) Kotobuki, M.; Leppelt, R.; Hansgen, D. A.; Widmann, D.; Behm, R. J. *J. Catal.* **2009**, *264*, 67–76.
(10) Lopez, N.; Janssens, T. V. W.; Clausen, B. S.; Xu, Y.; Mavrikakis, M.; Bligaard, T.; Nørskov, J. K. *J. Catal.* **2004**, *223*, 232–235.
(11) Janssens, T. V. W.; Clausen, B. S.; Hvolbæk, B.; Falsig, H.; Christensen, C. H.; Bligaard, T.; Nørskov, J. K. *Top. Catal.* **2007**, *44*, 15–26.
(12) Mavrikakis, M.; Stoltze, P.; Nørskov, J. K. *Catal. Lett.* **2000**, *64*, 101–106.
(13) Overbury, S. H.; Schwartz, V.; Mullins, D. R.; Yana, W.; Dai, S. *J. Catal.* **2006**, *241*, 56–65.
(14) Valden, M.; Lai, X.; Goodman, D. W. *Science* **1998**, *281*, 1647–1650.
(15) Chen, M. S.; Goodman, D. W. *Science* **2004**, *306*, 252–255.
(16) Chen, M. S.; Goodman, D. W. *Chem. Soc. Rev.* **2008**, *37*, 1860–1870.
(17) Herzing, A.; Kiely, C. J.; Carley, A. F.; Landon, P.; Hutchings, G. J. *Science* **2008**, *321*, 1331–1335.
(18) Zanella, R.; Giorgio, S.; Shin, C.-H.; Henry, C. R.; Louie, C. *J. Catal.* **2004**, *222*, 357–367.
(19) Tai, Y.; Yamaguchi, W.; Tajiri, K.; Kageyama, H. *Appl. Catal., A* **2009**, *364*, 143–149.
(20) Lemire, C.; Meyer, R.; Shaikhutdinov, S.; Freund, H.-J. *Angew. Chem., Int. Ed.* **2004**, *43*, 118–121.
(21) Herranz, T.; Deng, X.; Cabot, A.; Alivisatos, P.; Liu, Z.; Soler-Illia, G.; Salmeron, M. *Catal. Today* **2009**, *143*, 158–166.
(22) Valden, M.; Pak, S.; Lai, X.; Goodman, D. W. *Catal. Lett.* **1998**, *56*, 7–10.
(23) Lin, S. D.; Bollinger, M.; Vannice, M. A. *Catal. Lett.* **1993**, *17*, 245–262.

(24) Saint-Lager, M.-C.; Bailly, A.; Mantilla, M.; Garaudée, S.; Lazzari, R.; Dolle, P.; Robach, O.; Jupille, J.; Laoufi, I.; Taunier, P. *Gold Bull.* **2008**, *41*, 159–166.
(25) Saint-Lager, M.-C.; Bailly, A.; Dolle, P.; Baudoing-Savois, R.; Taunier, P.; Garaudée, S.; Cuccaro, S.; Douillet, S.; Geaymond, O.; Perroux, G.; Tissot, O.; Micha, J.-S.; Ulrich, O.; Rieutord, F. *Rev. Sci. Instrum.* **2007**, *78*, 083902–083910.
(26) Pan, J.-M.; Maschhoff, B. L.; Diebold, U.; Madey, T. E. *J. Vac. Sci. Technol., A* **1992**, *10*, 2470.
(27) Renaud, G.; Ducruet, M.; Ulrich, O.; Lazzari, R. *Nucl. Instrum. Methods Phys. Res., Sect. B* **2004**, *222*, 667–680.
(28) Jiang, P.; Porsgaard, S.; Borondics, F.; Köber, M.; Caballero, A.; Bluhm, H.; Besenbacher, F.; Salmeron, M. *J. Am. Chem. Soc.* **2010**, *132*, 2858–2859.
(29) Renaud, G.; Lazzari, R.; Leroy, F. *Surf. Sci. Rep.* **2009**, *64*, 255–380.
(30) Rauscher, M.; Paniago, R.; Metzger, T. H.; Kovats, Z.; Domke, J.; Pfannes, H. D.; Schulze, J.; Eisele, I. J. *Appl. Phys.* **1999**, *86*, 6763–6769.
(31) Lazzari, R. *J. Appl. Crystallogr.* **2002**, *35*, 406–421. http://www.insp.upmc.fr/axe2/Oxydes/IsGISAXS/isgisaxs.htm.
(32) Lazzari, R.; Renaud, G.; Jupille, J.; Leroy, F. *Phys. Rev. B* **2007**, *76*, 125412–125430.
(33) Hosemann, R.; Bagchi, S. N. *Direct Analysis of Diffraction by Matter*; North-Holland Publishing Company: Amsterdam, 1962.
(34) Pedersen, J. S.; Vysckocil, P.; Schonfeld, B.; Kostorz, G. *J. Appl. Crystallogr.* **1997**, *30*, 975–985.
(35) Diebold, U. *Surf. Sci. Rep.* **2003**, *48*, 53–229.
(36) Levine, J. R.; Cohen, J. B.; Chung, Y. W. *Surf. Sci.* **1991**, *248*, 215–224.
(37) Veith, G. M.; Lupine, A. R.; Pennycook, S. J.; Ownby, G. W.; Duney, J. *J. Catal.* **2005**, *231*, 151–158.
(38) Yang, F.; Chen, M. S.; Goodman, D. W. *J. Phys. Chem. C* **2009**, *113*, 254–260.
(39) Lai, X. T.; St Clair, P.; Valden, M.; Goodman, D. W. *Prog. Surf. Sci.* **1998**, *59*, 25–52.
(40) Zhang, L.; Cosandey, F.; Persaud, R.; Madey, T. E. *Surf. Sci.* **1999**, *439*, 73–85.
(41) Parker, S. C.; Grant, A. W.; Bondzie, V. A.; Campbell, C. T. *Surf. Sci.* **1999**, *441*, 10–20.
(42) Rashkeev, S. N.; Lupini, A. R.; Overbury, S. H.; Pennycook, S. J.; Pantelides, S. T. *Phys. Rev. B* **2007**, *76*, 035438.
(43) Cosandey, F.; Madey, T. E. *Surf. Rev. Lett.* **2001**, *8*, 73–93.
(44) Schumacher, B.; Denkwitz, Y.; Plzak, V.; Kinne, M.; Behm, R. J. *J. Catal.* **2004**, *224*, 449–462.
(45) Vijaykumar, T.; Raina, G.; Heun, S.; Kulkarni, G. U. *J. Phys. Chem. C* **2008**, *112*, 133111–133116.
(46) Hayden, B. E.; Pletcher, D.; Rendall, M. E.; Suchsland, J. P. *J. Phys. Chem. C* **2007**, *111*, 17044–17051.
(47) Hutchings, G. J.; Haruta, M. *Appl. Catal., A* **2005**, *291*, 2–5.